

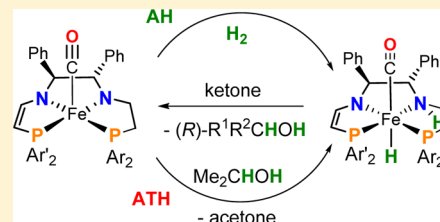
Iron Catalysts Containing Amine(imine)diphosphine P-NH-N-P Ligands Catalyze both the Asymmetric Hydrogenation and Asymmetric Transfer Hydrogenation of Ketones

Weiwei Zuo, Sebastian Tauer, Demyan E. Prokopchuk, and Robert H. Morris*

Department of Chemistry, University of Toronto, 80 Saint George St., Toronto, Ontario M5S3H6, Canada

S Supporting Information

ABSTRACT: When activated with base, the iron(II) complexes with tetradentate amine(imine)diphosphine ligands, (*S,S*)-*trans*-[FeCl(CO)(PAr₂-NH-N-PAr'₂)]BF₄ (1: Ar, Ar' = Ph; 2: Ar = Ph, Ar' = 4-MeC₆H₄; 3: Ar, Ar' = 3,5-Me₂C₆H₃), are very active for the asymmetric transfer hydrogenation (ATH) of ketones in KO^tBu/2-propanol. For ATH, better enantioselectivity, but lower catalytic activity, was observed in general when using catalyst precursors with the bulkier dixylylphosphino groups compared to those with diphenylphosphino groups. The complexes were much less active for the pressure hydrogenation of ketones, where 1 and 2 produced racemic product alcohols, while 3 yielded chiral alcohols with an enantiomeric excess of up to 70% (*R*) at turnover frequencies up to 80 h⁻¹ and turnover numbers of 100 for a range of ketones at 50 °C and 20 atm H₂. This is a rare example of asymmetric pressure hydrogenation using an iron complex. Unlike the case of ATH, there is no effect on the rate upon the addition of KO^tBu beyond the 2 equiv needed to convert the precursor complex to the active amido(ene-amido) and amine(ene-amido)hydrido forms. Both AH and ATH reactions share the same iron hydride intermediate formed by reaction of the amido(ene-amido) iron complex with either dihydrogen or 2-propanol. Kinetic studies on the H₂ hydrogenation of acetophenone catalyzed by 1, activated by base in benzene, using the method of initial rates indicated that the heterolytic splitting of the dihydrogen at the amido(ene-amido) iron complex is the turnover-limiting step of the catalytic cycle for hydrogenation. For 1 in benzene at 323 K over the ranges of concentrations [1] = (2.4–4.8) × 10⁻⁴ M and [ketone] = (3.6–7.2) × 10⁻² M, and of H₂ pressures = 10–20 atm, the rate law is rate = *k*[1][H₂], with *k* = 0.16 ± 0.01 M⁻¹ s⁻¹, Δ*H*[‡] = 10.0 ± 0.2 kcal mol⁻¹, and Δ*S*[‡] = -31.0 ± 0.5 cal mol⁻¹ K⁻¹. Detailed DFT calculations also support the finding that the barrier for H₂ splitting is the turnover-limiting step. The higher barrier for H₂ activation compared to isopropanol activation in order to generate the active amine(ene-amido)hydrido form explains why this system is biased toward ATH over AH.



INTRODUCTION

The asymmetric hydrogenation (AH) and asymmetric transfer hydrogenation (ATH) of prochiral ketones and imines are valuable transformations because they allow the production of enantiopure alcohols and amines for the use in the pharmaceutical, fragrance, food, and materials industries.¹ Previously, the predominant catalysts of these asymmetric transformations were based on rare and expensive metals such as ruthenium and rhodium. Replacing these precious metals with common metals such as iron has been the subject of significant investigations,² as iron is cheaper and potentially less toxic and more environmentally friendly.

As reviewed recently,^{2aa} we have developed catalysts based on iron(II) for the efficient asymmetric transfer hydrogenation of ketones and imines. The most effective catalysts contain a variety of amine–imine–diphosphine hybrid ligands (P-NH-N-P) (Chart 1).^{2x} Upon activation with 2–8 equiv of base, these imine–amine iron complexes showed exceptionally high catalytic activity in the hydrogenation of ketone substrates by transferring hydrogen from the 2-propanol solvent, with the highest TOF (turnover frequency) greater than 200 s⁻¹. The enantiomeric excesses (ee values) of the final chiral alcohols

and amines obtained from these iron catalysts are >99% for some substrates.

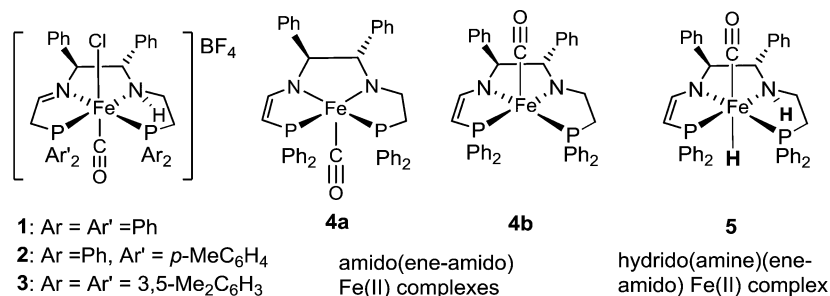
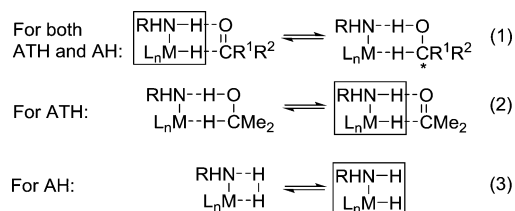
Iron amido(ene-amido) isomers (4a, 4b) and iron hydrido(amine)(ene-amido) (5) intermediates were characterized for the diphenylphosphino system (1), showing that the ATH catalysis proceeds by the outer sphere pathway shown in simplified form in Scheme 1.^{2q,s,x} First, the iron hydride amine complex attacks the ketone in the outer sphere (eq 1, Scheme 1), and then, the hydride amine is regenerated by reaction with 2-propanol (eq 2). We ask the question here whether the key iron hydride of eq 1 can be regenerated by reaction with hydrogen gas as in eq 3 so that the system can perform asymmetric hydrogenation (AH). Only a few AH catalysts based on iron have been reported.^{2c,k,y,z} The advantages of AH over ATH include the prevention of erosion of ee of the product observed sometimes for ATH, the use of higher

Special Issue: Catalytic and Organometallic Chemistry of Earth-Abundant Metals

Received: May 5, 2014

Published: June 13, 2014

Chart 1. Iron(II) P-NH-N-P Complexes for Asymmetric Transfer Hydrogenation and the Catalytically Active forms of 1

Scheme 1. General Equations for the ATH and AH of Prochiral Ketones Catalyzed by Metal Complexes with Ancillary Ligands L and Amine Ligand NH₂R

concentrations of ketone or imine substrate, and the economics of using hydrogen gas over other hydrogen donors.^{1b,3}

Certain ruthenium and osmium catalysts are thought to catalyze both ATH via eqs 1 and 2 and AH via eqs 1 and 3 (or similar ones involving additional alcohol or potassium alkoxide).^{3b,4} Others are strongly biased toward AH⁵ over ATH or can switch depending on the basicity of the system.⁶ Some ruthenium complexes without N-H groups catalyze both AH and ATH via other Ru-H routes.⁷ The factors that favor one type of catalysis over the other are still not well-defined.

We have done a small study of the effects of the substituents attached to the phosphorus atoms in catalyst precursors 1–3 on the enantioselectivity of ketone reduction and have found that the catalyst precursor (*S,S*)-3 with *meta*-xylyl groups on the phosphorus atoms provides higher ee values of (*R*)-1-phenylethanol and (*R*)-1-[3,5-bis(trifluoromethyl)phenyl]ethanol than the catalyst precursor 1 with diphenylphosphino groups.^{2n,x} In this report, we will describe further applications of these catalyst precursors in ATH as well as their reaction with H₂ and use in pressure AH reactions.

RESULTS

ATH of Ketones Catalyzed by 3. Our initial report on the applications of complexes 1–3 focused on the ATH of ketones mainly with complex 1.^{2x} Here, we report a comparison of results of ATH of ketone substrates of 3 vs 1 as catalyst precursors in basic 2-propanol at 28 °C (Table 1).

Generally, under the same conditions, precatalyst 3 exhibits lower activity than 1 for most substrates, as observed in the reduction of acetophenone. However, for 3-methyl-2-butanone, the rate of reaction was higher (entry 7 vs 8). The conversions except for α -tetralone were similar to those obtained by use of 1 as the catalyst does not shift the reaction equilibrium, but the enantiomeric excesses for most substrates were slightly superior to those obtained with 1. In each case, the same configuration (*R*) was obtained in excess using the (*S,S*)-catalyst. Of note, the α -tetralone can be converted into the corresponding alcohol with much higher enantioselectivity and with little deterioration

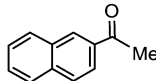
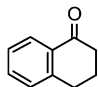
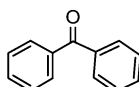
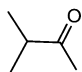
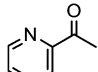
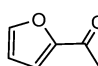
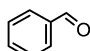
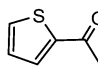
of ee (entry 3 vs 4). The enantiomeric excess of (*R*)-1-(2-pyridinyl)ethanol was increased by 19% by use of 3 (entry 9 vs 10). The exception was the reduction of 3-methyl-2-butanone to 3-methyl-2-butanol with higher catalytic activity, but lower enantioselectivity (entry 7 vs 8).

Asymmetric Pressure Hydrogenation of Ketones. The H₂ hydrogenation of ketone substrates catalyzed by iron catalysts was conducted by first reacting the precatalysts (1–3) with KO^tBu in THF in the glovebox to form the amido(ene-amido) iron complexes, followed by injecting the THF solutions of the catalysts to the reactor that was charged with H₂ and THF solution of the substrate. Full conversion of acetophenone at a turnover number (TON) of 100 was achieved in 4.5 h for 1 at 20 atm and 50 °C (Table 2, entry 1; Figure S1, Supporting Information).

However, the products obtained with catalysts containing phenyl and *para*-tolyl substituents on the phosphine atoms (1 and 2) are racemic (Table 2, entries 1–5). Decreasing the temperature or lowering the hydrogen pressure led to a decrease of the TOF with still no enantioselectivity (entries 2 and 3). At higher temperature, the reduction of acetophenone occurs faster and it takes a shorter time for the completion of the reaction (entry 4). The use of other solvents that do not react with the amido(ene-amido) iron complex (benzene, hexane, triethylamine) gave similar results as that in THF, whereas using dichloromethane and *tert*-butyl alcohol led to deactivation of the catalysis. The *R*-isomer of 1-phenylethanol is produced in 35% ee after 1 h of reaction (18% conversion) by use of the enantioselective precatalyst 3 having *meta*-xylyl substituents. Unfortunately, the erosion of the enantiomeric excess continues as the reaction continues until racemic products are finally obtained. Unlike the case of transfer hydrogenation,^{2x} the presence of excess base (more than 2 equiv) has no clear influence on the activity and enantioselectivity (entry 6 vs entry 7). As in the transfer hydrogenation, the reduction of 3,5-bis(trifluoromethyl)acetophenone provided a higher ee value for the chiral product (entry 11) than that of acetophenone (entry 6). A much lower catalytic activity was observed in the reduction of α -tetralone, but the enantioselectivity was good (entry 12). Interestingly, as in the case of transfer hydrogenation, the ee of the 1-tetralol product did not drop with time.

In order to understand the mechanistic details of this iron-catalyzed H₂ hydrogenation of ketones, the reaction of the amido(ene-amido) iron complex with H₂ was studied in an attempt to identify the potential amine iron hydride intermediate. The reaction of 1 with 2 equiv of base and followed by reaction with H₂ at 20 atm in THF at room temperature for 30 min produces a mixture of an amine iron

Table 1. Asymmetric Transfer Hydrogenation of Ketones^{a,b,c}

entry	substrate	Cat. Precur.	time (s)/conv. (%)/ TON (at equil.)	TOF (s ⁻¹) at 50% conv.	ee (%) (<i>R</i>) at 10 s/ at equil.	Ref.
1	2-acetonaphthone	3	180/83/5030	160	86/82	This work
2		1	180/84/5140	158	92/83	2x
3	α -tetralone	3	5400/29/1700	0.3 ^b	89 ^c /85	This work
4		1	600/73/4470	4	34/33	2x
5	benzophenone	3	600/88/5400	27	-	This work
6		1	600/88/5400	38	-	2x
7	3-methyl-2-butanone	3	1800/89/5440	10	36/31	This work
8		1	3600/67/4100	3	57/54	2x
9	2-acetyl pyridine	3	360/96/5870	38	43/43	This work
10		1	360/98/6000	100	25/24	2x
11	2-acetyl furan	3	480/82/5000	35	43/33	This work
12		1	360/84/5140	61	51/31	2x
13	benzaldehyde	3	60/91/5550	104	-	This work
14		1	25/99/6060	242	-	2x
15	2-acetyl-thiophene	3	1800/51/3150	2	49/45	This work
16		1	360/51/3150	10	50/40	This work

^aGeneral conditions: [Catalyst] = 6.73×10^{-5} M, [KO^tBu] = 5.45×10^{-4} M, [substrate] = 0.412 M, [2-PrOH] = 12.4 M, 28 °C. ^bThe TOF at 29% conversion. ^cAt 60 s, since early times gave unreliable ee due to the small conversion.

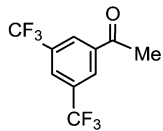
hydride complex **5** and a neutral amido(ene-amido) iron complex **4a** in a 4:3 ratio (Scheme 2).

A doublet of doublet hydride ¹H NMR pattern at -2.3 ppm (²J_{HP} = 70.0 and 70.8 Hz; see Figure S2, Supporting Information) and the chemical shifts of the protons in the P-NH-N-P ligand are exactly the same as those found in the product of the reaction of **1** with base and 2-propanol (Figure 1).^{2x} The IR (KBr pellet) spectrum of the reaction mixture also shows a CO stretch at 1872 cm⁻¹ for the amine hydride complex and 1906 cm⁻¹ for the amido(ene-amido) complex **4a**. This unstable iron hydride slowly isomerized in C₆D₆ to another hydride compound in the absence of substrate; this observation was also reported for the hydride species in the ATH mechanism.^{2x} Furthermore, both of the two hydride species react with acetophenone in C₆D₆ to produce 1-phenylethanol. It was also found that the ratio of the hydride complex to the unreacted amido(ene-amido) iron complex was not significantly affected by either the reaction time or the reaction temperature, although, under higher reaction temper-

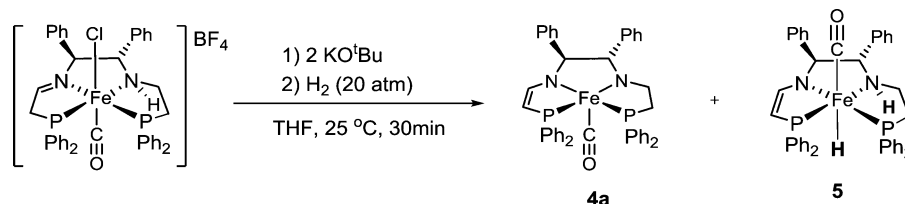
atures (50 °C), the hydride complex easily decomposes in the absence of a ketone substrate.

Kinetics of H₂ Hydrogenation Reactions Catalyzed by 1. The kinetic studies on the H₂ hydrogenation of acetophenone catalyzed by **1** were conducted by the initial rate method in benzene. The linear formation of 1-phenylethanol as a function of time was plotted for a series of different concentrations of acetophenone, H₂, and catalyst and different temperatures. The reactions were initiated by injecting a catalyst solution in benzene of a small volume into the reactor that was charged with H₂ and acetophenone dissolved in benzene. To make sure that the temperature inside the reactor was the same as that of the outside water bath, the benzene solution of acetophenone was pre-equilibrated at the preset temperature for more than 30 min prior to the injection of the catalyst solution. The catalyst solution was prepared by reacting **1** with base in THF initially in the glovebox, followed by evaporating THF under reduced vacuum and extracting the product with benzene. The reactions were sampled at timed

Table 2. Asymmetric Pressure H₂ Hydrogenation of Ketones^a

entry	substrate	precatalyst	base (equiv.)	temp (°C)	H ₂ (atm)	TOF (h ⁻¹) at 1 h	ee (%) at 1 h (<i>R</i>)	time (h) for full conversion
1	acetophenone	1	2	50	20	40	racemic	4.5
2	acetophenone	1	2	25	20	10	racemic	15
3	acetophenone	1	2	50	10	20	racemic	10
4	acetophenone	1	2	70	20	60	racemic	2.5
5	acetophenone	2	2	50	20	80	racemic	1.5
6	acetophenone	3	2	50	20	18	35	10
7	acetophenone	3	4	50	20	18	35	10
8	acetophenone	3	2	70	20	33	29	6
9	acetophenone	3	2	50	10	8	35	15
10	2-acetonaphthone	3	2	50	20	18	32	10
11	3,5-bis(trifluoromethyl)acetophenone	3	2	50	20	20	55	10
								
12	α-tetralone	3	2	50	20	3	70	60

^aConditions: [Catalyst] = 3.48×10^{-4} M, [substrate] = 3.48×10^{-2} M in THF (30 mL), S/C = 100.

Scheme 2. Dihydrogen Activation by the Amido(ene-amido) Iron Complex Generated in Situ by Reaction of 1 with KO^tBu

intervals, and the degree of conversion was determined by gas chromatography (GC) analysis. The dependence of initial rates on the reaction parameters together with the reaction conditions is shown in Figures 2–5 and Table 3.

The initial rate of 1-phenylethanol formation is first-order in catalyst concentration and H₂ pressure but independent of the ketone concentration. This is indicative of a turnover-limiting dihydrogen splitting step in the catalytic cycle, consistent with that of our previous ruthenium catalysts,^{5b} but in contrast to the Knölker's iron complex where the hydrogen transfer from the iron hydride to the carbonyl group is the rate-limiting step.⁸ Therefore, the rate law at 323 K for the range of ketone, catalyst, and H₂ concentrations studied is given by eq 4, where the rate constant is $k = 0.16 \pm 0.01 \text{ M}^{-1} \text{ s}^{-1}$, assuming that all the catalyst precursors were converted to the active species.

$$\text{rate} = d[\text{alcohol}]/dt = -d[\text{ketone}]/dt = k[\text{cat.}][\text{H}_2] \quad (4)$$

The activation parameters obtained from an Eyring plot of the data of Table 3 (see the Supporting Information) will be compared with those calculated by DFT as discussed below.

Density Functional Theory (DFT) Calculations on the Mechanism of AH with 1. We have demonstrated in a previous DFT study^{2s} that the mechanism of ATH using simplified models of **4b** and **5** (Scheme 2) involves stepwise proton/hydride transfer from FeH–NH complex **5** to

acetophenone. On the basis of the calculated relative free energies, this was postulated to be the turnover-limiting step when isopropanol is used as the reductant. The hydride (FeH–NH) and alkoxide (Fe(OCHMePh)–NH) compounds were found to be the lowest-energy species, acting as possible resting states in the catalytic cycle. Thus, once the FeH–NH complex is formed in solution, as shown in Scheme 2, we expect that the same mechanism is operational to reduce ketonic substrates, with the only difference now being that H₂ gas is responsible for regenerating the FeH–NH complex. Since H₂ splitting was found to be the turnover-limiting step during catalysis, our focus will be on calculating H₂ splitting barriers using a simplified version of complex **5** and comparing this with the calculated energies of the full system **5**, which includes all of the phenyl substituents.

We have calculated the barrier for H₂ splitting on the same simplified amido-eneamido system, using the same level of theory as in our previous work^{2s} and also using the M06-L functional with the TZVP/TZVPfit basis set (see the Experimental Section). The latter functional/basis set combination was shown to be an efficient and accurate method in comparing thermochemical values between theory and experiment for other organometallic transformations.¹⁰ In addition, solvation effects were taken into account by using a THF solvent continuum. Scheme 3 shows that the H₂ splitting barriers for both functional/basis set combinations are

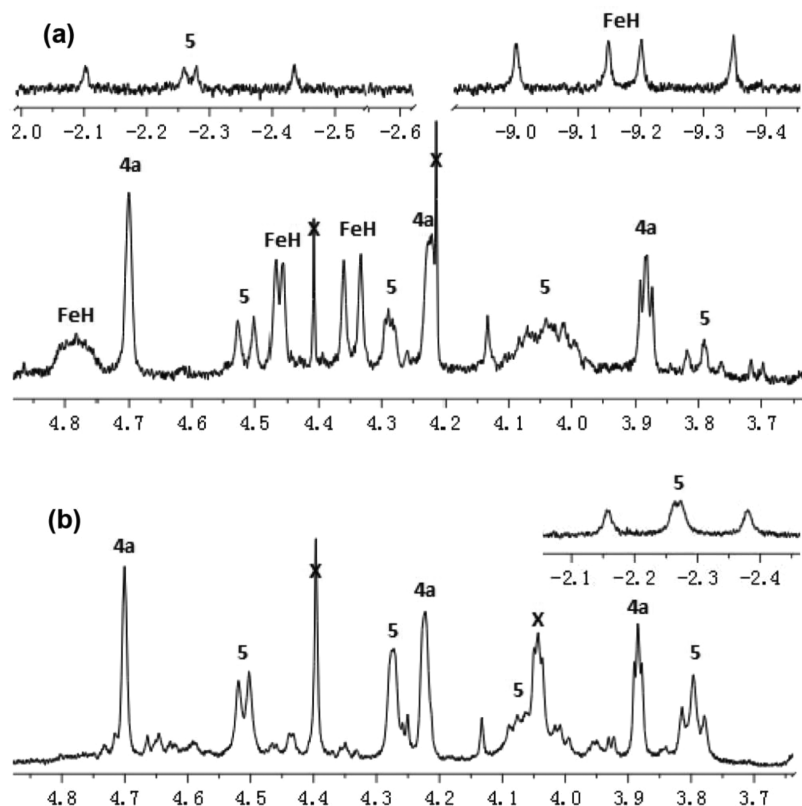


Figure 1. (a) The ^1H NMR (400 MHz, C_6D_6) spectrum of the products of the reaction of **1**, base, and 2-propanol in 2-propanol.^{2x} (b) The ^1H NMR (600 MHz, C_6D_6) spectrum of the reaction of **1**, base, and H_2 at 20 atm in THF. In (a) and (b), the signals at δ 4.5, 4.3, 4.0 (broad), and 3.8 ppm along with hydride resonances at δ -2.3 ppm (dd) correspond to protons of the amine iron hydride complex **5**, while the resonances at δ 4.7, 4.2, and 3.9 ppm originate from the neutral amido(ene-amido) complex **4a**, and the signal at δ 4.4 ppm is H_2 gas. The other major signals along with hydride resonances at δ -9.2 ppm (dd) in (a) belong to a second amine iron hydride complex that forms more slowly (FeH).^{2x}

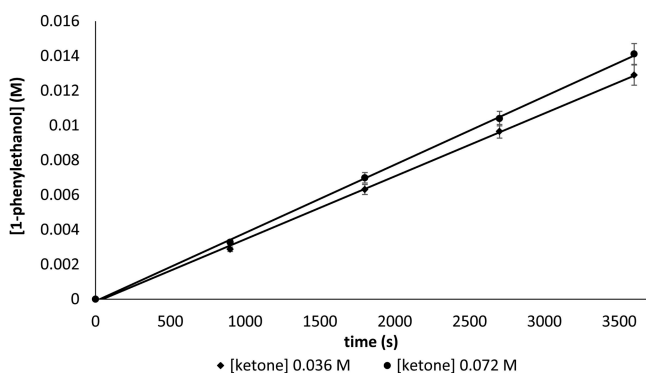


Figure 2. Dependence of initial rate on the acetophenone concentration. Conditions: $[\text{acetophenone}] = 3.6 \times 10^{-2}$ and 7.2×10^{-2} M and $[\text{catalyst}] = 3.6 \times 10^{-4}$ M in benzene (30 mL); H_2 pressure = 20 atm; temperature = 50°C .

comparable ($G^\ddagger(\text{TS}_{4b\text{H},5b\text{H}}) = 17.2$ vs 18.0 kcal/mol), with the relative free energies differing by only 0.8 kcal/mol relative to **4b_H** plus all relevant small molecules. Formation of the FeH-NH complex **5b_H** is exergonic by 9.0 kcal/mol (M06/6-31++G(d,p)) and 7.1 kcal/mol (M06-L/TZVP/TZVPfit), respectively. The metrical parameters for $\text{TS}_{4b\text{H},5b\text{H}}$ are very similar using both levels of theory, and the structure is presented in Figure 6.

We were also interested in optimizing structures and obtaining H_2 splitting barriers using a full structural analogue of **1**, which included (S,S)-dpen and all phenyl substituents on

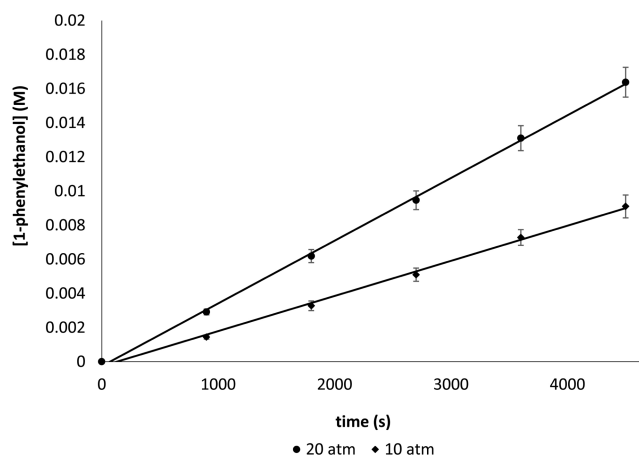


Figure 3. Dependence of initial rate on the H_2 pressure. Conditions: $[\text{acetophenone}] = 3.6 \times 10^{-2}$ M; $[\text{catalyst}] = 3.6 \times 10^{-4}$ M in benzene; temperature = 50°C ; H_2 pressure = 10, 20 atm.

phosphorus. As noted earlier, M06-L/TZVP/TZVPfit (see the Experimental Section) was found to be an energetically accurate functional/basis set combination for organometallic systems, with efficient optimization times, even on complete systems incorporating cyclohexyl- and phenylphosphine ligands.¹⁰ Thus, for all further calculations discussed, we chose to use M06-L/TZVP/TZVPfit to optimize ground-state and transition-state structures.

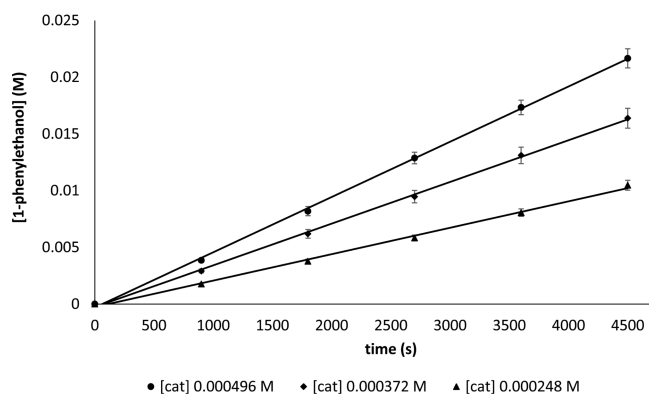


Figure 4. Dependence of initial rate on the catalyst concentration. Conditions: [acetophenone] = 3.6×10^{-2} M; [catalyst] = 2.4, 3.6, and 4.8×10^{-4} M in benzene; H_2 pressure = 20 atm; temperature = 50 °C.

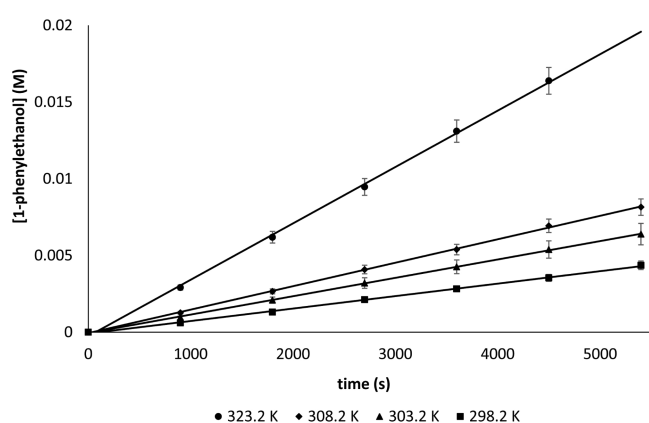


Figure 5. Dependence of initial rate on the temperature. Conditions: [acetophenone] = 3.6×10^{-2} M, [catalyst] = 3.6×10^{-4} M in benzene; H_2 pressure = 20 atm; temperature = 25, 30, 35, and 50 °C.

When **1** reacts with 2 equiv of base, two enantiomers form in solution (**4a** and **4b**), where the carbonyl ligand is located on either side of the PNNP ligand plane (Scheme 4).^{2x} Simplified complex **4b_H**, as discussed above, is structurally analogous to **4b**. Using molecule **4a** as our free energy reference point, along with all relevant small molecules, we wanted to investigate why H_2 splitting selectively occurred with complex **4b**, leaving **4a** untouched (Scheme 2).

First, coordination of H_2 to **4a** successfully leads to optimization of the η^2-H_2 complex **4aH₂**, which is 13.8 kcal/mol higher in energy than **4a**. Carefully inspecting the orientation of the amide ligand of **4aH₂** reveals that the nitrogen lone pair is pointing away from the η^2-H_2 ligand

(Figure 7), similar to the orientation of the NH group in complex **1**.

Our attempts at trying to find an H_2 splitting transition state between **4aH₂** and the FeH–NH complex **5a** were unsuccessful. In order for heterolytic H_2 splitting to occur across the metal–amide moiety, the nitrogen atom must orient its electron pair toward the σ^* molecular orbital of hydrogen. The pyramidal inversion at nitrogen might be too energetically unfavorable, since the hydrogen atoms on the alkyl groups attached to nitrogen are in a diaxial position; pyramidal inversion would then require the entire ligand system to reorient itself in order to relieve this diaxial strain (Scheme 4). Calculations were performed where the ligand is initially reoriented to relieve this unfavorable diaxial interaction, but attempts to find both an η^2-H_2 ground-state structure and an H_2 splitting transition state were also unsuccessful (see the Supporting Information). Furthermore, the energy of the FeH–NH complex **5a** ($G^\circ = 5.5$ kcal/mol) is substantially higher than the free energies of **4b_H** and **5b** (vide infra).

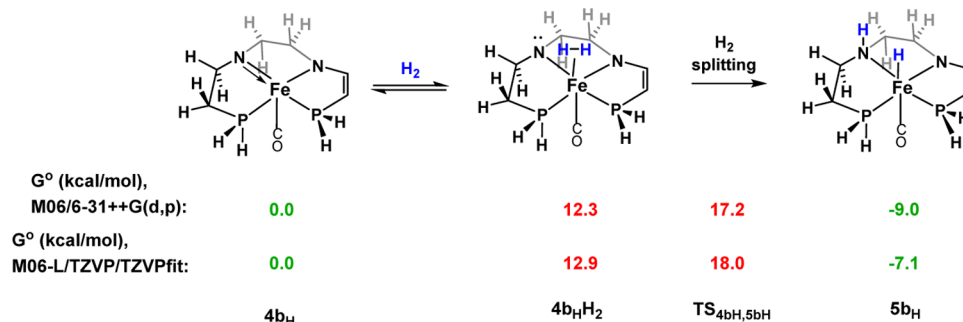
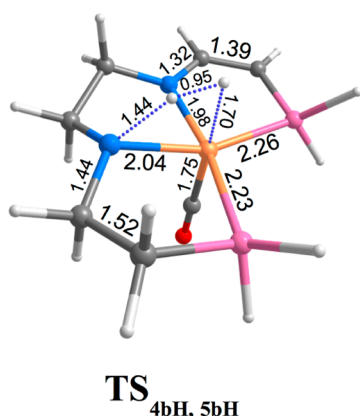
Starting with complex **4b** ($G^\circ = -1.4$ kcal/mol relative to **4a**), an η^2-H_2 ground state was found (**4bH₂**), which is only about 0.5 kcal/mol lower in energy than **4aH₂**. However, in this case, the amide lone pair is oriented on the same side as coordinated dihydrogen. Comparing bond length pairs in **4aH₂** and **4bH₂** (Figure 7) reveals that there is little difference between the two structures, but there is obviously a dramatic difference in the orientation of the P–N_{amido} portion of the ligand with respect to coordinated dihydrogen. From **4bH₂**, an H_2 splitting transition state was found ($\Delta G^{\ddagger}(\text{TS}_{4b,5b} - \mathbf{4b}) = 17.5$ kcal/mol), generating hydride complex **5b**, which is exergonic by 6.9 kcal/mol (when compared with amido(ene-amido) compound **4b**). The calculated structure of **TS_{4b,5b}** is shown in Figure 7, and bond lengths are strikingly similar to its simplified analogue **TS_{4bH,5bH}** (Figure 6).

We were also interested to know why complexes **1–3** do not exhibit the same activity and enantioselectivity for ATH and AH. Table 4 lists the calculated and experimentally measured activation parameters (ΔG^{\ddagger} , ΔH^{\ddagger} , ΔS^{\ddagger}) in both ATH and AH, relative to the free energy of amido(ene-amido) complex **4b_H** for ATH and **4a** for AH. The relative free energies (G°) in ATH for the turnover-limiting step (hydride transfer to acetophenone from **5b_H**) were taken from our previous experimental^{2q} and theoretical^{2s} studies on the mechanism of transfer hydrogenation using these amido(ene-amido) systems. Table 4 clearly shows that the experimental and calculated H_2 splitting free energy barrier for AH are both higher than the turnover-limiting step for ATH and that there is good agreement between the experiment and theory for the case of AH.

Table 3. Observed and Calculated (eq 4) Rates of Reactions

entry	[Fe] (M)	temp (K)	[H ₂] ^a (atm/M)	[ketone] (M)	rate (v_0) (M s ^{−1})	$k = v_0/([Fe][H_2])$ (M ^{−1} s ^{−1})
1	3.6×10^{-4}	323	$20/6.1 \times 10^{-2}$	3.6×10^{-2}	3.6×10^{-6}	0.16 ± 0.01
2	3.6×10^{-4}	323	$20/6.1 \times 10^{-2}$	7.2×10^{-2}	3.7×10^{-6}	0.17 ± 0.01
3	3.6×10^{-4}	323	$10/3.0 \times 10^{-2}$	3.6×10^{-2}	1.8×10^{-6}	0.17 ± 0.01
4	2.4×10^{-4}	323	$20/6.1 \times 10^{-2}$	3.6×10^{-2}	2.2×10^{-6}	0.15 ± 0.01
5	4.8×10^{-4}	323	$20/6.1 \times 10^{-2}$	3.6×10^{-2}	4.7×10^{-6}	0.16 ± 0.01
6	3.6×10^{-4}	298	$20/5.4 \times 10^{-2}$	3.6×10^{-2}	8.3×10^{-7}	0.043 ± 0.004
7	3.6×10^{-4}	303	$20/5.6 \times 10^{-2}$	3.6×10^{-2}	1.2×10^{-6}	0.060 ± 0.005
8	3.6×10^{-4}	308	$20/6.0 \times 10^{-2}$	3.6×10^{-2}	1.6×10^{-6}	0.074 ± 0.007

^aThe H_2 concentration in benzene was calculated using Henry's law based on the data of ref 9.

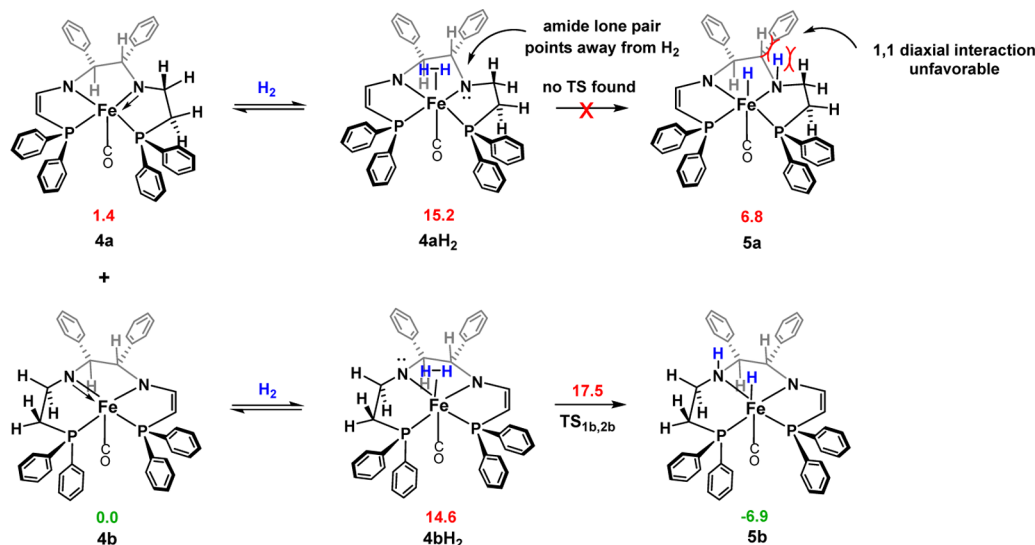
Scheme 3. Calculated Structures Starting with Simplified Amido(ene-amido) Complex **4b_H** (1 atm, 298 K)^a^aRelative free energies (G°) are presented in kcal/mol.**Figure 6.** Calculated structure of **TS_{4bH,5bH}** ($\nu = 1074i$). Distances are in angstroms (Å).

DISCUSSION

Asymmetric pressure hydrogenation of ketones catalyzed by iron complexes is rare, but recently, a family of enantioselective catalysts with TOF up to 2000 h⁻¹ at 50 °C and 5 atm H₂ have been reported. There is also a recent report of less active (TOF

up to 50 h⁻¹ at 45 °C, 50 atm H₂), but highly enantioselective, catalysts generated in situ using Fe₃(CO)₁₂ and a macrocyclic phosphorus nitrogen ligand.²² The current systems have activities comparable to the latter group but are not as enantioselective. Nevertheless, they are interesting because a comparison between ATH and AH can be made due to their well-defined kinetics.

We propose that catalysis proceeds mainly via the cycle shown in Scheme 5. This cycle accounts for our spectroscopic observation of the conversion of **1** to produce the amido(ene-amido) isomers **4a** and **4b** and the reaction of **4b** with dihydrogen (or with isopropanol in ATH) to give the reactive dihydride **5**. The structure and role of the dihydride **5** in ATH have already been elucidated, and this complex in the (*S,S*) configuration is known to react with prochiral ketones enantioselectively and rapidly at room temperature to give alcohols in the (*R*) configuration with high ee.^{2x} This sense of enantioinduction is also observed when (*S,S*)-**3** is used as a catalyst for ATH or AH. This simplified cycle does not explain why the precursors **1** and **2** give alcohols in high ee for ATH, at least under the short reaction times (minutes),^{2x} but racemic products for AH, in reaction times of hours at room temperature. The as yet uncharacterized side reactions that

Scheme 4. Calculated Structures Starting with Amido(ene-amido) Complex **4a** or **4b** (1 atm, 298 K)^a^aRelative free energies (G°) are presented in kcal/mol. Conformational isomers of **4b** and **4bH₂** have also been calculated, but these conformers do not facilitate η^2 -H₂ coordination or H₂ splitting (see the Supporting Information).

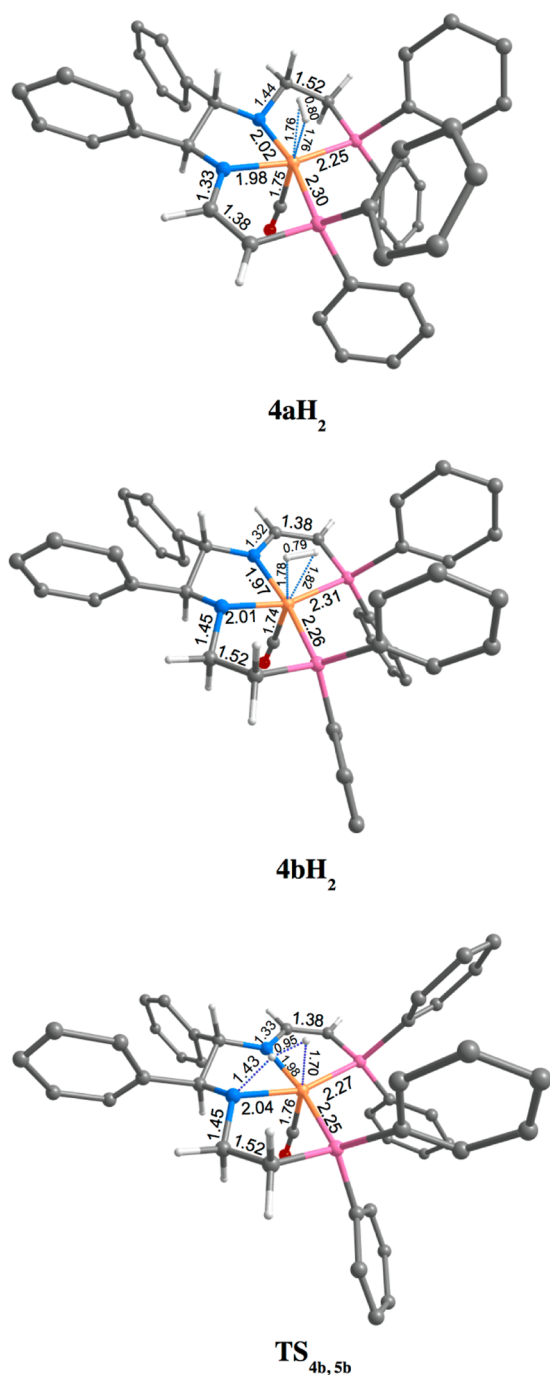
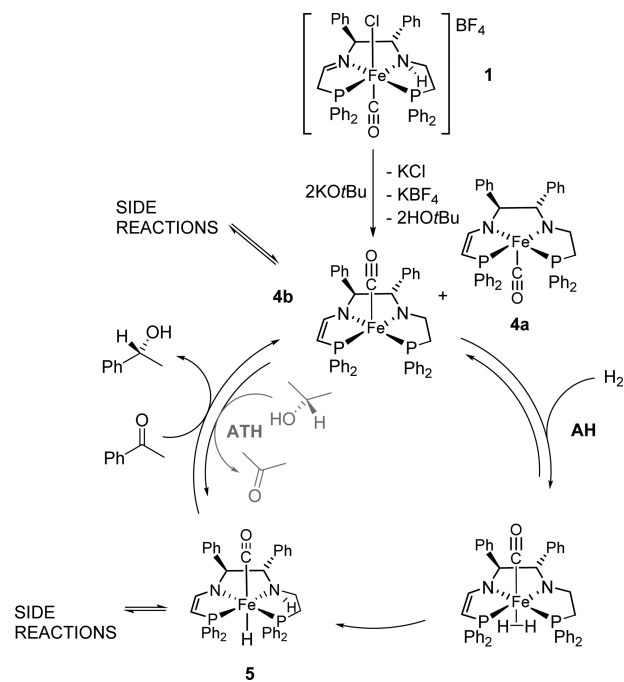


Figure 7. Calculated structures of **4aH₂**, **4bH₂**, and **TS_{4b,5b}** ($\nu = 1089i$). Distances are in angstroms (Å). Phenyl hydrogens have been omitted for clarity.

Scheme 5. Proposed Simplified Mechanism for the Major AH Catalytic Cycle (in Black) and the Mechanism for ATH (in Gray)



lead to a second hydride species and possibly alkoxide complexes, as well as the role of the apparently less reactive amido(ene-amido) complex **4a**, still need to be clarified. Side reactions with alcohols are clearly important since the current work has shown that AH is suppressed by use of *tert*-butanol as the solvent. In addition, an isopropoxide complex was calculated to be of comparable energy to the hydride **5**.^{2s}

This cycle along with DFT calculations helps to explain why these iron catalyst systems are biased toward ATH over AH. The barrier for the formation of the reactive hydride **5** is higher for AH than ATH. The reaction of amido(ene-amido) with dihydrogen is calculated to have a barrier of 16 kcal/mol, whereas that with isopropanol is 12 kcal/mol (Table 4). The experimentally determined barrier for the former is 20 kcal/mol at 50 °C and 20 atm, although side reactions, currently under investigation, might be responsible for the discrepancy between experiment and theory.

CONCLUSIONS

In addition to being a highly efficient catalyst for the asymmetric transfer hydrogenation of ketones, the amine(imine)diphosphine iron complexes also catalyze the H₂ hydrogenation of ketone substrates with low activity and

Table 4. Comparison of Experimental and Calculated (from DFT) Activation Parameters for Hydride Transfer to Acetophenone in ATH Relative to **4b_H**, and H₂ Splitting in AH Relative to **4b^a**

parameter	ATH ^b exptl.	ATH ^c calcd.	AH ^d exptl.	AH ^d calcd.
ΔH^{\ddagger} (kcal/mol)	6.0 ± 0.2	−3	10.0 ± 0.2	7
ΔS^{\ddagger} (cal/mol·K)	-28 ± 1	−48	-31.0 ± 0.5	−29
ΔG^{\ddagger} (kcal/mol)	14.3 ± 0.5	12	20.0 ± 0.5	16

^aATH calculations are at the M06/6-31++G(d,p) level of theory with isopropanol solvent continuum, and AH calculations are at the M06-L/TZVP/TZVPfit level of theory with tetrahydrofuran solvent continuum. ^bReference 2q. There are potentially large errors associated with these data due to the multiparameter kinetic modeling involved and the difficulty in separating the kinetics of catalyst activation from the kinetics of the catalytic cycle.

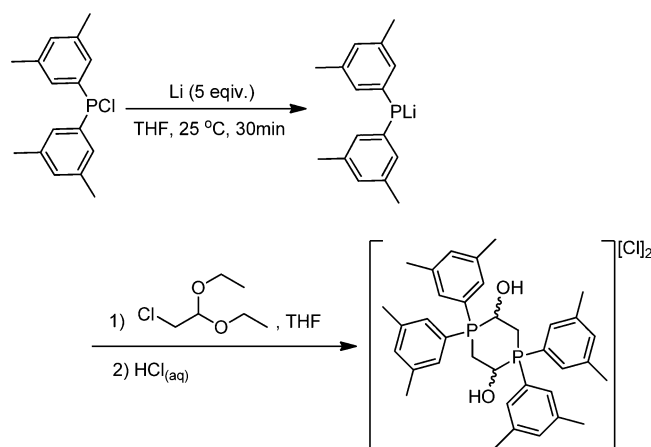
^cReference 2s. ^d20 atm, 323 K.

enantioselectivity. The same structure of the amine iron hydride intermediate formed by reacting the amido(ene-amido) iron complex with dihydrogen as that obtained by reacting with 2-propanol suggests a similar reaction mechanism in both hydrogenation reactions. The zero-order of reaction rate on the ketone concentration and the first-order on the H_2 pressure and catalyst concentration indicate that the heterolytic splitting of dihydrogen across the polar iron–nitrogen double bond is the turnover-limiting step in AH, an observation supported by detailed DFT calculations. The system is biased toward ATH over AH because the barrier for isopropanol addition to the iron amido species (Scheme 1, eq 2) is a lower-energy process than addition of dihydrogen (Scheme 1, eq 3). In contrast to the case of transfer hydrogenation catalysis, the base concentration has no effect on the hydrogenation rate and enantioselectivity when the number of equivalents of the base relative to the precatalyst is greater than a 2:1. Further investigation into the role of the base, the side reactions that lead to lower rates and enantioselectivity for catalytic hydrogenation, and changes in catalyst design in order to obtain more efficient H_2 hydrogen catalysts are ongoing in our lab.

EXPERIMENTAL SECTION

General Considerations. All procedures and manipulations involving air-sensitive materials were performed under an argon or nitrogen atmosphere using Schlenk techniques or a glovebox with nitrogen or argon. Solvents were degassed and dried using standard procedures prior to all manipulations and reactions. The catalyst precursors 1–3 were synthesized following our previous procedure.^{2x} Acetophenone and liquid ketone substrates were distilled under argon and stored under molecular sieves in a glovebox prior to reduction reaction, while the solid substrates were purified by sublimation. Deuterated solvents were purchased from Cambridge Isotope Laboratories and distilled and dried over activated molecular sieves. All of the other reagents used in the procedures were purchased from commercial sources and utilized without further purification. NMR spectra were recorded at ambient temperature and pressure using Varian Gemini 600, 400, and 300 MHz spectrometers [1H (600, 400, and 300 MHz), $^{13}C\{^1H\}$ (150, 100, and 75 MHz), and $^{31}P\{^1H\}$ (242, 161, and 121 MHz)]. The ^{31}P NMR spectra were referenced to 85% H_3PO_4 (0 ppm). Elemental analyses were performed using a PerkinElmer 2400 CHN elemental analyzer at the Department of Chemistry at the University of Toronto. The electrospray ionization mass spectrometry (ESI-MS) data were collected on an AB/Sciex QStar mass spectrometer with an ESI source.

All DFT calculations were performed using Gaussian 09 (Revision B.01 or D.01).¹¹ Two different combinations of density functionals and basis sets were used: M06¹²/6-31++G(d,p)¹³ (only for complexes **4b_H**, **4b_HH₂**, **TS_{4bH,5bH}**, and **5b_H**) or M06-L¹⁴/TZVP¹⁵ (also known as def-TZVP) with the TZVPfit density fitting basis set. Either normal (opt) or tight (opt = tight) convergence criteria were used for all optimizations, and a pruned (99 590) integration grid was used throughout (grid = ultrafine). Optimizations were performed in tetrahydrofuran (THF) solvent using the integral equation formalism polarizable continuum model (IEF-PCM)¹⁶ with radii and non-electrostatic terms from the SMD solvation model (scrf = smd).¹⁷ Full vibrational and thermochemical analyses (1 atm, 298 K) were performed on optimized structures to obtain solvent-corrected free energies (G°) and enthalpies (H°). For direct comparison of activation parameters between calculated and experimental species (Table 4), the freqchk utility was used (20 atm, 323 K) to obtain solvent-corrected free energies (G°) and enthalpies (H°). Optimized ground states were found to have zero imaginary frequencies, while transition states had exactly one imaginary frequency. Open-shell optimizations were not considered in this study. Three-dimensional visualizations of calculated structures were generated by ChemCraft.¹⁸



Synthesis of the Cyclic Phosphonium Dimers with *meta*-Xylyl Substituents at the Phosphorus Atoms.

In an argon glovebox, a THF (50 mL) solution of bis(3,5-dimethylphenyl)-phosphine chloride (1.30 g, 4.70 mmol) was added to lithium powder (0.16 g, 23.5 mmol) in a round-bottom flask charged with a stirring bar. The resultant mixture was stirred at 25 °C for 30 min with the formation of a red solution. The dark red solution was then filtered via a sintered glass crucible to remove a black precipitate. Chloroacetaldehyde diethyl acetal (0.72 g, 4.70 mmol) was added, and the mixture was stirred at 25 °C overnight. The flask was taken out of the glovebox, and diluted hydrochloric acid (10 mL, 1.17 M) was added. The mixture was stirred overnight to cause the white precipitate. The white suspension was filtered to obtain a white solid, and the solution was discarded. The white solid was washed with water (20 mL) by stirring the suspension for more than 3 h. The white suspension was filtered to obtain a white solid, which was further washed with a 1:1 mixture of hexane/ethyl acetate. The final product was dried under vacuum for more than 12 h. Yield: 1.2 g, 80%. Two diastereomers in a ratio of 4:5 were observed. For the major isomer: 1H NMR (400 MHz, $CDCl_3$ + 2 drop CD_3OD) δ : 2.30 (s, 12H, CH_3), 3.64 (m, 2H, CH_2), 3.96 (m, 2H, CH_2), 5.91 (m, 2H, $CHOH$), 7.23 (m, ArH), 7.43 (m, ArH), 7.51 (m, ArH), 7.57 (m, ArH). $^{13}C\{^1H\}$ NMR (100 MHz; $CDCl_3$ + 2 drop CD_3OD) δ : 21.0 (s, CH_3), 21.1 (s, CH_3), 23.5 (d, J_{CP} = 42.0 Hz, PCH_2), 61.6 (d, J_{CP} = 65.7 Hz, $PCHOH$), 115.7 (d, J_{CP} = 83.1 Hz, ArC), 116.7 (d, J_{CP} = 81.8 Hz, ArC), 129.6 (d, J_{CP} = 9.6 Hz, ArC(o)), 130.5 (d, J_{CP} = 9.9 Hz, ArC(o)), 136.9 (d, J_{CP} = 3.1 Hz, ArC(p)), 137.4 (d, J_{CP} = 2.9 Hz, ArC(p)), 140.0 (d, J_{CP} = 13.8 Hz, ArC(m)), 141.2 (d, J_{CP} = 13.2 Hz, ArC(m)). $^{31}P\{^1H\}$ NMR (161 MHz; $CDCl_3$ + 2 drop CD_3OD) δ : 11.8. For the minor isomer: 1H NMR (400 MHz, $CDCl_3$ + 2 drop CD_3OD) δ : 2.27 (s, 6H, CH_3), 2.28 (s, 6H, CH_3), 3.64 (m, 2H, CH_2 , overlap with the major isomer), 3.96 (m, 2H, CH_2 , overlap with the major isomer), 6.00 (m, 2H, $CHOH$), 7.23 (m, ArH, overlap with the major isomer), 7.43 (m, ArH, overlap with the major isomer), 7.51 (m, ArH, overlap with the major isomer), 7.57 (m, ArH, overlap with the major isomer). $^{13}C\{^1H\}$ NMR (100 MHz; $CDCl_3$ + 2 drop CD_3OD) δ : 21.0 (s, CH_3), 21.1 (s, CH_3), 23.3 (d, J_{CP} = 47.0 Hz, PCH_2), 61.4 (d, J_{CP} = 66.4 Hz, $PCHOH$), 114.7 (d, J_{CP} = 80.9 Hz, ArC), 115.5 (d, J_{CP} = 82.5 Hz, ArC), 129.5 (d, J_{CP} = 10.0 Hz, ArC(o)), 130.4 (d, J_{CP} = 10.0 Hz, ArC(o)), 137.0 (s, ArC(p)), 137.4 (s, ArC(p)), 140.4 (d, J_{CP} = 13.6 Hz, ArC(m)), 140.8 (d, J_{CP} = 13.9 Hz, ArC(m)). $^{31}P\{^1H\}$ NMR (161 MHz; $CDCl_3$ + 2 drop CD_3OD) δ : 14.3. FT-IR (KBr, cm^{-1}): 561w, 690s, 864s, 953m, 1071s, 1139s, 1215w, 1270s, 1380m, 1420s, 1440s, 1600s, 2865s, 2920s, 2989s, 3028s, 3368s. HRMS (ESI-TOF, MeOH/ CH_2Cl_2 = 1:1) m/z calculated for $[C_{18}H_{22}OP]^+$ 285.1408, found: 285.1406; calculated for methanol adduct $[C_{19}H_{26}O_2P]^+$ 317.1671, found: 317.1674. Anal. Calcd for $C_{36}H_{44}Cl_2O_2P_2 \cdot H_2O$: C, 65.53; H, 7.03. Found: C, 65.62; H, 7.20.

Preparation of Complex 3. This complex was synthesized as reported, and the spectroscopic properties were identical.^{2x} Anal. Calcd for $C_{51}H_{56}BClF_4N_2OP_2Fe$: C, 64.24; H, 5.92; N, 2.94. Found: C, 63.92; H, 5.94; N, 2.84.

General Procedure for the Asymmetric Transfer Hydrogenation of Ketone Substrates Using 3 as the Catalyst Precursor. For comparison with 1 and 2, the reaction conditions for the asymmetric transfer hydrogenation of acetophenone and other ketone substrates catalyzed by 3 were kept the same as our previous standard conditions.²⁹ The final concentrations of the reagents were adjusted to be as follows [ketone] = 0.412 M, [3] = 6.73×10^{-5} M, [KO^tBu] = 5.45×10^{-4} M, and [iPrOH] = 12.4 M. The quantity of the precatalyst for each single catalytic reaction was measured via a stock solution method. A concentrated stock solution was made by dissolving complex 3 (19 mg, 0.0197 mmol) in 6.08 g of cold dichloromethane. After all the solids were dissolved, the solution was immediately sucked into a syringe. The solution was then divided into several equal portions in several vials such that each portion has 0.2 g of the stock solution, and then dichloromethane was evaporated to obtain a yellow solid. These operations led to a precatalyst quantity of 6.48×10^{-7} mol in each vial. The base was prepared by dissolving KO^tBu (10 mg, 0.089 mmol) in iPrOH (1.02 g, 1.30 mL). These solutions were used only after all the solids were completely dissolved and for less than 2 days. iPrOH (6.63 g, 8.44 mL), the ketone substrate (3.95×10^{-3} mol), and a clean stirring bar were added to the vial that contains the precatalyst, and the solution was stirred for several minutes until all the precatalysts were dissolved. A 0.06 g portion of the base stock solution (5.24×10^{-6} mol of base, 8 equiv) was added into a vial that contains 0.501 g of iPrOH, and the mixed solution was then added into the above solution to initiate the catalytic reaction. The samples were taken by injecting small portions of the reaction mixture into septa-sealed GC vials containing aerated 2-propanol for efficient quenching of the reaction. Samples were analyzed using a PerkinElmer Autosystem XL chromatograph with a chiral column (CP chiral-Dex CB 25 m \times 2.5 mm). Hydrogen gas was used as a mobile phase at a column pressure of 5 psi. The injector temperature was 250 °C, and the FID temperature was 275 °C. The amount of 1-phenylethanol in the sample was determined relative to the amount of the acetophenone.

General Procedure for the High-Pressure H₂ Hydrogenation of Ketone Substrates Using 1–3 as the Catalyst Precursors. Hydrogenation reactions were carried out at constant pressures of H₂ using a stainless steel 50 mL Parr hydrogenation reactor. The temperature was maintained using a constant temperature water bath. The reactor was flushed several times with hydrogen gas at 5 atm prior to the addition of substrate and catalyst. For a standard catalysis, the catalyst was generated by first reacting the precatalysts (0.01 mmol) with KO^tBu (0.02–0.04 mmol) in THF (5 mL) in the glovebox to form the amido(ene-amido) iron complex. A THF (25 mL) solution of the substrate (1 mmol) was injected into the reactor via a syringe equipped with a 12 in. needle under a hydrogen flow of 5 atm. This solution was pre-equilibrated in a water bath at a preset temperature for more than 30 min. The catalysis was initiated by injecting the catalyst solution into the reactor with rigorous stirring under a hydrogen flow of 5 atm, followed by adjusting the H₂ pressure to the preset value. Small aliquots of the reaction mixture were sampled at regular time intervals from a stainless-steel sampling dip tube attached to a modified Parr reactor. The dip tube was 30 cm in length with an inner diameter of 0.01 in., and a swing valve was attached to the end of the sampling tube. Samples were analyzed using a PerkinElmer Autosystem XL chromatograph with a chiral column (CP chiral-Dex CB 25 m \times 2.5 mm). Hydrogen gas was used as a mobile phase at a column pressure of 5 psi. The injector temperature was 250 °C, and the FID temperature was 275 °C. The amount of 1-phenylethanol in the sample was determined relative to the amount of the acetophenone. For the catalysis carried out in other solvents, the real catalyst was still generated in THF in the glovebox. THF was then removed under vacuum, and the employed solvent (5 mL) was added to extract the amido(ene-amido) iron complex. Other procedures were the same as above. A typical reaction profile in terms of formation of 1-phenylethanol with time catalyzed by 1 and 2 equiv of base in THF is shown in Figure S1 (Supporting Information).

Dihydrogen Activation by the Amido(ene-amido) Iron Complex Generated in Situ by Reaction of 1 with KO^tBu. A

vial in the argon glovebox was charged with 1 (100 mg, 1.20 mmol) and KO^tBu (27.0 mg, 2.40 mmol), and THF (25 mL) was added. The reaction mixture was allowed to stir at room temperature for 10 min to yield a dark blue solution. The THF solution was transferred via a syringe equipped with a 12 in. needle under a hydrogen flow of 5 atm to a stainless steel 50 mL Parr hydrogenation reactor that was flushed several times with hydrogen gas prior to use. The H₂ pressure was adjusted to 20 atm, and the solution was stirred at room temperature for 30 min. The pressure was reduced to 5 atm, and the product solution was sucked into a syringe equipped with a 12 in. needle under a hydrogen flow of 5 atm. This solution was then transferred into a Schlenk flask that was charged with inert gas. The solvent was removed under vacuum, and the product was extracted with C₆D₆ for NMR analysis. The ¹H NMR spectrum (600 MHz, C₆D₆) indicated the presence of two major products: the amine iron hydride 5 and the amido(ene-amido) complex 4a. For 5: δ : -2.25 (dd, ²J_{HP} = 70.0 and 70.8 Hz, FeH), 3.80 (dd, J_{HH} = 10.8 Hz, J_{HH} = 11.4 Hz, 1H, CH(Ph)NH), 4.00 (m, NH), 4.35 (dd, J_{HP} = 2.2 Hz, J_{HH} = 4.4 Hz, 1H, PCH), 4.52 (d, J_{HH} = 10.8 Hz, CH(Ph)N). FT-IR (KBr, cm⁻¹): 1523 ($\nu_{\text{NCH=CHP}}$), 1872 (ν_{CO}), 3500 (ν_{NH}). For 4a: δ : 3.89 (dd, J_{HP} = 3.7 Hz, J_{HH} = 3.7 Hz, 1H, PCH), 4.22 (m, 1H, CH(Ph)), 4.70 (m, 1H, CH(Ph)). FT-IR (KBr, cm⁻¹): 1906.

Kinetics. The above hydrogenation catalysis procedure was utilized for the kinetic study except that the solvent was benzene.

■ ASSOCIATED CONTENT

■ Supporting Information

A typical reaction profile in terms of formation of 1-phenylethanol with time catalyzed by 1 in THF; the ¹H NMR spectrum of the product from the reaction of 1, base, and 20 atm H₂; and the Eyring plot for the calculation of activation parameters. This material is available free of charge via the Internet at <http://pubs.acs.org>.

■ AUTHOR INFORMATION

Corresponding Author

*E-mail: rmorris@chem.utoronto.ca.

Notes

The authors declare no competing financial interest.

■ ACKNOWLEDGMENTS

NSERC Canada is thanked for a Discovery Grant to R.H.M. and a Doctoral Scholarship to D.E.P. The Deutscher Akademischer Austauschdienst (DAAD) is thanked for support for S.T. The Canadian Foundation for Innovation, project number 19119, and the Ontario Research Fund provided funding of the Centre for Spectroscopic Investigation of Complex Organic Molecules and Polymers.

■ REFERENCES

- (1) (a) Huang, Y.; Liu, N.; Wu, X.; Che, Y. *Curr. Org. Chem.* **2010**, *14*, 1447–1460. (b) Blaser, H.-U.; Pugin, B.; Spindler, F. *Top. Organomet. Chem.* **2012**, *42*, 65–102. (c) Dupau, P. In *Organometallics as Catalysts in the Fine Chemical Industry*; Beller, M., Blaser, H. U., Eds.; Springer-Verlag: Berlin, 2012; Vol. 42, pp 47–63. (d) Magano, J.; Dunetz, J. R. *Org. Proc. Res. Dev.* **2012**, *16*, 1156–1184. (e) Palmer, A. M.; Zanotti-Gerosa, A. *Curr. Opin. Drug Discovery Dev.* **2010**, *13*, 698–716. (f) Blaser, H. U. *Top. Catal.* **2010**, *53*, 997–1001. (g) Saudan, L. A. *Acc. Chem. Res.* **2007**, *40*, 1309–1319. (h) Ikariya, T.; Blacker, A. J. *Acc. Chem. Res.* **2007**, *40*, 1300–1308. (i) Noyori, R. *Adv. Synth. Catal.* **2003**, *345*, 15–32.
- (2) (a) Chen, J. S.; Chen, L. L.; Xing, Y.; Chen, G.; Shen, W. Y.; Dong, Z. R.; Li, Y. Y.; Gao, J. X. *Acta Chim. Sin. (Huaxue Xuebao)* **2004**, *62*, 1745–1750. (b) Nishiyama, H.; Furuta, A. *Chem. Commun.* **2007**, 760–762. (c) Sui-Seng, C.; Freutel, F.; Lough, A. J.; Morris, R. H. *Angew. Chem., Int. Ed.* **2008**, *47*, 940–943. (d) Mikhailine, A. A.

- Lough, A. J.; Morris, R. H. *J. Am. Chem. Soc.* **2009**, *131*, 1394–1395.
- (e) Tondreau, A. M.; Darmon, J. M.; Wile, B. M.; Floyd, S. K.; Lobkovsky, E.; Chirik, P. J. *Organometallics* **2009**, *28*, 3928–3940.
- (f) Meyer, N.; Lough, A. J.; Morris, R. H. *Chem.—Eur. J.* **2009**, *15*, 5605–5610.
- (g) Morris, R. H. *Chem. Soc. Rev.* **2009**, *38*, 2282–2291.
- (h) Hosokawa, S.; Ito, J.; Nishiyama, H. *Organometallics* **2010**, *29*, 5773–5775.
- (i) Naik, A.; Maji, T.; Reiser, O. *Chem. Commun.* **2010**, 46, 4475–4477.
- (j) Zhou, S.; Fleischer, S.; Junge, K.; Das, S.; Addis, D.; Beller, M. *Angew. Chem., Int. Ed.* **2010**, *49*, 8121–8125.
- (k) Berkessel, A.; Reichau, S.; von der Hoh, A.; Leconte, N.; Neudorfl, J. M. *Organometallics* **2011**, *30*, 3880–3887.
- (l) Flückiger, M.; Togni, A. *Eur. J. Org. Chem.* **2011**, 4353–4360.
- (m) Lagaditis, P. O.; Lough, A. J.; Morris, R. H. *J. Am. Chem. Soc.* **2011**, *133*, 9662–9665.
- (n) Sues, P. E.; Lough, A. J.; Morris, R. H.; Salnuovo Al, V. P. *Organometallics* **2011**, *30*, 4418–4431.
- (o) Fleischer, S.; Werkmeister, S.; Zhou, S. L.; Junge, K.; Beller, M. *Chem.—Eur. J.* **2012**, *18*, 9005–9010.
- (p) Hopewell, J. P.; Martins, J. E. D.; Johnson, T. C.; Godfrey, J.; Wills, M. *Org. Biomol. Chem.* **2012**, *10*, 134–145.
- (q) Mikhailine, A. A.; Maishan, M. I.; Lough, A. J.; Morris, R. H. *J. Am. Chem. Soc.* **2012**, *134*, 12266–12280.
- (r) Mikhailine, A. A.; Maishan, M. I.; Morris, R. H. *Org. Lett.* **2012**, *14*, 4638–4641.
- (s) Prokopchuk, D. E.; Morris, R. H. *Organometallics* **2012**, *31*, 7375–7385.
- (t) Sonnenberg, J. F.; Coombs, N.; Dube, P. A.; Morris, R. H. *J. Am. Chem. Soc.* **2012**, *134*, 5893–5899.
- (u) Yu, S.; Shen, W.; Li, Y.; Dong, Z.; Xu, Y.; Li, Q.; Zhang, J.; Gao, J. *Adv. Synth. Catal.* **2012**, *354*, 818–822.
- (v) Fleischer, S.; Zhou, S. L.; Werkmeister, S.; Junge, K.; Beller, M. *Chem.—Eur. J.* **2013**, *19*, 4997–5003.
- (w) Gopalaiah, K. *Chem. Rev.* **2013**, *113*, 3248–3296.
- (x) Zuo, W.; Li, Y.; Lough, A. J.; Morris, R. H. *Science* **2013**, *342*, 1080–1083.
- (y) Lagaditis, P. O.; Sues, P. E.; Sonnenberg, J. F.; Wan, K. Y.; Lough, A. J.; Morris, R. H. *J. Am. Chem. Soc.* **2014**, *136*, 1367–1380.
- (z) Li, Y.; Yu, S.; Wu, X.; Xiao, J.; Shen, W.; Dong, Z.; Gao, J. *J. Am. Chem. Soc.* **2014**, *136*, 4031–4039.
- (aa) Sues, P. E.; Demmans, K. Z.; Morris, R. H. *Dalton Trans.* **2014**, 43, 7650–7667.
- (3) (a) Verzijl, G. K. M.; De Vries, A. H. M.; De Vries, J. G.; Kapitan, P.; Dax, T.; Helms, M.; Nazir, Z.; Skranc, W.; Imboden, C.; Stichler, J.; Ward, R. A.; Abele, S.; Lefort, L. *Org. Process Res. Dev.* **2013**, *17*, 1531–1539.
- (b) Rautenstrauch, V.; Hoang-Cong, X.; Churlaud, R.; Abdur-Rashid, K.; Morris, R. H. *Chem.—Eur. J.* **2003**, *9*, 4954–4967.
- (c) Naud, F.; Malan, C.; Spindler, F.; Ruggeberg, C.; Schmidt, A. T.; Blaser, H. U. *Adv. Synth. Catal.* **2006**, *348*, 47–50.
- (4) (a) Clapham, S. E.; Hadzovic, A.; Morris, R. H. *Coord. Chem. Rev.* **2004**, *248*, 2201–2237.
- (b) O, W. N. O.; Lough, A. J.; Morris, R. H. *Organometallics* **2011**, *30*, 1236–1252.
- (c) Sandoval, C. A.; Li, Y. H.; Ding, K. L.; Noyori, R. *Chem.—Asian J.* **2008**, *3*, 1801–1810.
- (d) Hadzovic, A.; Song, D.; MacLaughlin, C. M.; Morris, R. H. *Organometallics* **2007**, *26*, 5987–5999.
- (e) Baratta, W.; Fanfoni, L.; Magnolia, S.; Siega, K.; Rigo, P. *Eur. J. Inorg. Chem.* **2010**, 1419–1423.
- (f) Baratta, W.; Chelucci, G.; Magnolia, S.; Siega, K.; Rigo, P. *Chem.—Eur. J.* **2009**, *15*, 726–732.
- (g) Baratta, W.; Ballico, M.; Del Zotto, A.; Siega, K.; Magnolia, S.; Rigo, P. *Chem.—Eur. J.* **2008**, *14*, 2557–2563.
- (h) Baratta, W.; Ballico, M.; Chelucci, G.; Siega, K.; Rigo, P. *Angew. Chem., Int. Ed.* **2008**, *47*, 4362–4365.
- (5) (a) Ohkuma, T.; Ooka, H.; Hashiguchi, S.; Ikariya, T.; Noyori, R. *J. Am. Chem. Soc.* **1995**, *117*, 2675–2676.
- (b) Abdur-Rashid, K.; Clapham, S. E.; Hadzovic, A.; Harvey, J. N.; Lough, A. J.; Morris, R. H. *J. Am. Chem. Soc.* **2002**, *124*, 15104–15118.
- (c) Sandoval, C. A.; Ohkuma, T.; Muniz, K.; Noyori, R. *J. Am. Chem. Soc.* **2003**, *125*, 13490–13503.
- (6) Ohkuma, T.; Utsumi, N.; Tsutsumi, K.; Murata, K.; Sandoval, C.; Noyori, R. *J. Am. Chem. Soc.* **2006**, *128*, 8724–8725.
- (7) (a) Ito, J.; Ujiie, S.; Nishiyama, H. *Organometallics* **2009**, *28*, 630–638.
- (b) Kayaki, Y.; Ikeda, H.; Tsurumaki, J. I.; Shimizu, I.; Yamamoto, A. *Bull. Chem. Soc. Jpn.* **2008**, *81*, 1053–1061.
- (c) Vicente, C.; Shulpin, G. B.; Moreno, B.; Sabo-Etienne, S.; Chaudret, B. *J. Mol. Catal. A: Chem.* **1995**, *98*, L5–L8.
- (d) Menashe, N.; Salant, E.; Shvo, Y. *J. Organomet. Chem.* **1996**, *514*, 97–102.
- (8) Casey, C. P.; Guan, H. *J. Am. Chem. Soc.* **2007**, *129*, 5816–5817.
- (9) Yong, C. L., Ed. *Hydrogen and Deuterium; Solubility Data Series*; Pergamon Press: New York, 1981; Vols. 5/6.
- (10) Gusev, D. G. *Organometallics* **2013**, *32*, 4239–4243.
- (11) Frisch, M. J.; et al. *Gaussian 09*, Rev. B.01 and rev. D.01; Gaussian, Inc.: Wallingford, CT, 2009. For the full reference, see the Supporting Information.
- (12) (a) Zhao, Y.; Truhlar, D. *Theor. Chem. Acc.* **2008**, *120*, 215–241.
- (b) Zhao, Y.; Truhlar, D. G. *Acc. Chem. Res.* **2008**, *41*, 157–167.
- (13) (a) Frisch, M. J.; Pople, J. A.; Binkley, J. S. *J. Chem. Phys.* **1984**, *80*, 3265–3269.
- (b) Hariharan, P. C.; Pople, J. A. *Theor. Chem. Acc.* **1973**, *28*, 213–222.
- (c) Hehre, W. J.; Ditchfield, R.; Pople, J. A. *J. Chem. Phys.* **1972**, *56*, 2257–2261.
- (d) Krishnan, R.; Binkley, J. S.; Seeger, R.; Pople, J. A. *J. Chem. Phys.* **1980**, *72*, 650–654.
- (14) Zhao, Y.; Truhlar, D. G. *J. Phys. Chem.* **2006**, *125*, 194101.
- (15) Schäfer, A.; Huber, C.; Ahlrichs, R. *J. Chem. Phys.* **1994**, *100*, 5829–5835.
- (16) (a) Tomasi, J.; Mennucci, B.; Cammi, R. *Chem. Rev.* **2005**, *105*, 2999–3094.
- (b) Tomasi, J.; Mennucci, B.; Cancès, E. *J. Mol. Struct.: THEOCHEM* **1999**, *464*, 211–226.
- (17) Marenich, A. V.; Cramer, C. J.; Truhlar, D. G. *J. Phys. Chem. B* **2009**, *113*, 6378–6396.
- (18) <http://www.chemcraftprog.com>.